ONBOARD DOPPLER COMPENSATION FOR LOW-RATE COMMUNICATIONS OVER COMMERCIAL RELAY SATELLITES

Adam Gannon
NASA Glenn Research Center, Cleveland, OH, USA
adam.gannon@nasa.gov, +1 216 433 2926
Joseph Downey
NASA Glenn Research Center, Cleveland, OH, USA 44135
joseph.a.downey@nasa.gov, +1 216 433 6067
Mick Koch
NASA Glenn Research Center, Cleveland, OH, USA 44135
mick.v.koch@nasa.gov, +1 216 433 2866

Abstract

NASA spacecraft performing scientific and exploration missions may increasingly communicate over commercial relay satellites, including those that operate at Ka-band. Ideally these spacecraft could use the same Ka-band terminal for low-rate telemetry/commanding. However, this use case presents an issue since most commercial relay systems were designed with terrestrial users in mind and cannot easily handle the Doppler effects of orbiting spacecraft. In this work we propose onboard Doppler compensation allowing spacecraft to use existing relay satellite infrastructure without modification. Specifically, we present a method for digital compensation based on a series of piecewise linear sweeps which minimizes resources used on the spacecraft's radio. We perform orbital mechanics simulations to estimate the worst-case Doppler profiles experienced by spacecraft in several low-Earth orbits. We emulate these effects in a laboratory experiment and demonstrate the proposed technique will reduce Doppler effects by more than two orders of magnitude. The residual Doppler is small enough that modems used at commercial relay sites are able to receive error-free data even when operating at their lowest supported symbol rate.

1 Introduction

Future spacecraft will communicate across a multitude of civil and commercial relay providers, enabled by waveform-agile software-defined radios featuring front-ends with a wide tunable frequency range [1, 2]. This ecosystem will augment, and eventually replace, the Tracking and Data Relay Satellite System (TDRSS) operated by the National Aeronautics and Space Administration (NASA). From its conception, TDRSS was designed for spacecraft communications and provides Doppler compensation as an optional yet integrated service. However, many commercial relay satellite networks were designed to serve terrestrial users whose relative velocities are many orders of magnitude less than spacecraft. At low symbol rates, Doppler shifts due to dynamics of Earth-orbiting spacecraft are potentially too large for carrier tracking loops in off-the-shelf receivers to compensate for unaided. This is particularly true for Ka-band (26.5 – 40 GHz) signals used by many commercial relay satellite systems.

A crucial capability TDRSS provides is continuous global coverage for commanding and telemetry. This latter type of traffic frequently operates at relatively low rates (kbps) for saving power or increasing link margin to ensure delivery of crucial data. Though these low-rate links are sometimes accomplished with a separate communications system, we consider a mass-saving scenario in which a user spacecraft has a single Ka-band system for both high-rate and low-rate communications. Support for this low-rate use case, particularly important in off-nominal conditions, must continue as NASA spacecraft increasingly operate with commercial systems. However, NASA benefits most from working with existing commercial systems – as one customer among many. Increased sophistication on the spacecraft side can prevent the need for major modifications to commercial relay satellite networks to support this use case.

In Section 2 we bound the range of Doppler effects experienced by typical Earth-orbiting spacecraft. A characterization of modems used by commercial relays in Section 3 informs us of the minimum symbol rate modems can lock to using their own carrier recovery loops (without compensation). Section 4 presents our spacecraft-side compensation technique. Our design emphasis is to reduce utilization of the spacecraft radio's field-programmable gate array (FPGA), which can be highly resource constrained. Sources of error in this technique and their corrections are analyzed in Section 5. Finally, experimental results from laboratory testing are presented in Section 6. We show the technique can reduce residual Doppler to within the tracking capability of commercial modems, allowing error-free data transfer down to the lowest rate (250 kbaud) supported by the modems.

2 Doppler Characteristics

The fractional shift due to the Doppler effect is

$$\gamma = \frac{\Delta f_c}{f_c} = \frac{v_r \cos \alpha}{c} \tag{1}$$

where $\alpha \in [0, \pi]$ is the angle of the velocity vector from user spacecraft to relay satellite, v_r is the magnitude of relative velocity, and $c = 3 \times 10^8$ m/s is the speed of light. This fractional shift will equally affect the carrier frequency $\Delta f_c = \gamma f_c$ and symbol timing $\Delta R_s = \gamma R_s$.

2.1 On-Orbit Statistics

We consider a user spacecraft with two representative ephemerides in low-Earth orbit (LEO):

- A 400km medium inclination (51°) orbit used by the International Space Station (ISS).
- A 500km sun-synchronous orbit (SSO) at 85° inclination, a popular satellite orbit.

For field of view calculations, the user terminal is assumed to have a zenith-facing steerable dish antenna in the 1m class, yielding a half power beamwidth of approximately 0.8°. As demonstrated in [1], it is possible for a single terminal to cover the entire 17.7 - 31 GHz frequency range used by Ka-band space relays. For relay orbits, we consider both geostationary (GEO) and medium-Earth (MEO) orbits, which are used by operational relay satellite systems. As representative relays we base our analysis on the Global Xpress and O3b constellations for GEO and MEO, respectively. For MEO we assume a 45° field of view which is used by the O3b constellation [3]. We assume the GEO field of view is wide enough to cover the entirety of LEO.

Fig. 1 shows statistics gathered from an orbital mechanics simulation over a one year analysis period. For each contact from the user spacecraft to a relay, we calculated the maximum Doppler shift as a fraction (in parts per million) of the carrier frequency. Also included is the Doppler experienced by the link from the MEO relay to its ground station on Earth. The total Doppler experienced during a MEO contact will be the sum of the user-relay and relay-Earth Doppler shifts, though the former is dominant. Depending on position of the user, the two Doppler shift components may interfere constructively or destructively. Doppler on the relay-Earth link from a GEO satellite is negligible.

2.2 Worst-Case Profiles

From the simulation we generated a worst-case Doppler profile. We used the approximate frequencies of Global Xpress and O3b as representative examples. For MEO, we aligned the profiles of the user-relay and relay-Earth links such that the greatest composite Doppler shift is generated. As shown in Fig. 2a, this produces an asymmetry about the y-axis. As will be discussed in Section 3, modem performance depends not just on the Doppler shift but also the rate of change in the Doppler shift (hereafter *Doppler*

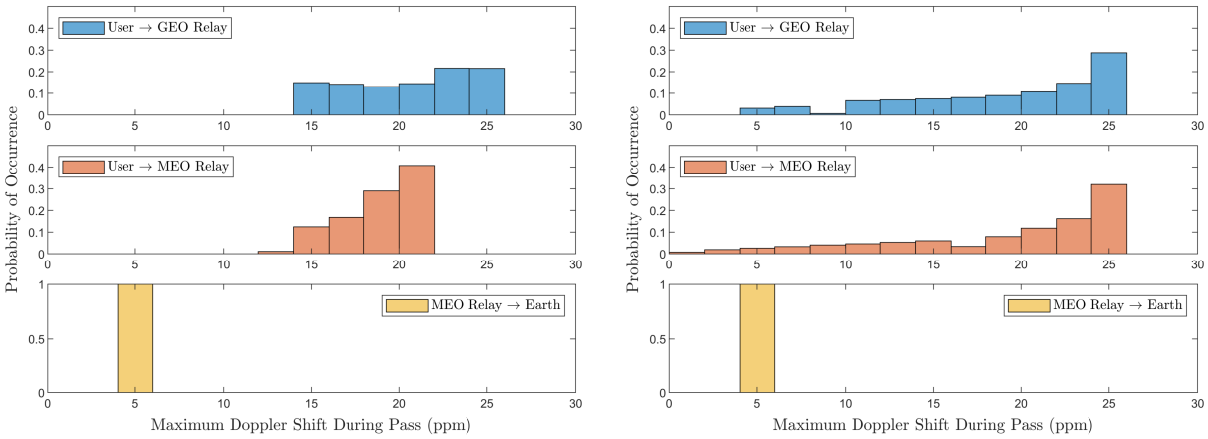

Figure 1: Maximum Doppler shift (in parts per million) experienced during a pass expressed as a percentage of total passes from (a) ISS and (b) SSO. Statistics calculated over one simulated year.

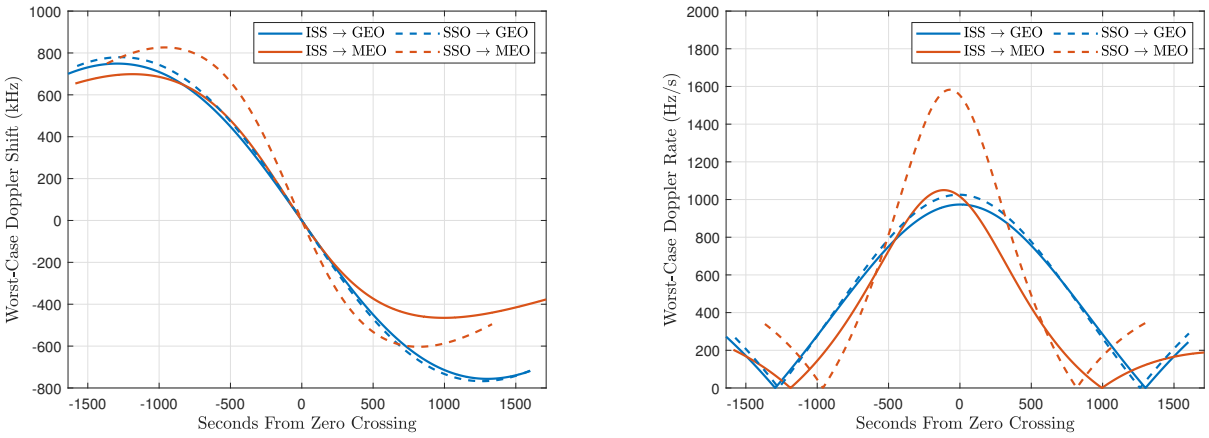

Figure 2: Doppler profile of worst-case passes showing Doppler (a) shift and (b) rate.

rate). As we can see in Fig. 2b, MEO experiences less of a total Doppler shift than GEO but has a worse Doppler rate.

Doppler also effects symbol timing. However, even the worst-case value in Fig. 1 of γ = 25 ppm is much less than the typical $R_S/100$ bandwidth of a receiver's timing recovery process such as a Gardner loop. We consider it likely the timing recovery can easily handle uncorrected timing error due to Doppler and do not consider symbol timing compensation in this design.

3 Modem Characterization

Next, we determined the Doppler performance of commercial relays without spacecraft-side compensation. We selected three modems known to be used at ground stations supporting operational relay satellites. All modems support the 2nd generation Digital Video Broadcast - Satellite (DVB-S2) standard which has been successfully used between ISS and GEO relays [4]. Our spacecraft side was emulated by a software-defined radio (SDR) implemented on a Vadatech μTCA chassis with a NASA-developed DVB-S2 transmitter design. Tests were performed using QPSK 1/2, believed to be a representative choice for low-rate communications due to minimal signal-to-noise ratio requirements. Pilots were enabled to aid synchronization.

Fig. 3 shows the test setup for evaluating modem Doppler performance. Profiles, such as in Fig. 2a, are fed to an RT Logic channel simulator which emulates Doppler in the link. A noise generator is used to add variable levels of white Gaussian noise to achieve a target 3 dB link margin relative to the quasi-error free threshold in the DVB-S2 standard [5]. A high-accuracy (<5 ppb) rubidium frequency reference was distributed to all devices to maximize the likelihood that errors would be due to Doppler effects alone.

To characterize Doppler shift, a static frequency offset was generated by the channel emulator. The transmitter was turned on and the modems given 60 seconds to lock, as indicated by consistent increase of error-free frames. The shift was then increased by a small amount and the process repeated until the modem failed to lock. Ten trials were run at each symbol rate. Fig. 4a shows the result of shift characterization for the three modems. Note that testing in this manner tracks acquisition. Once acquired, modems may be able to track a larger shift than in Fig. 4a.

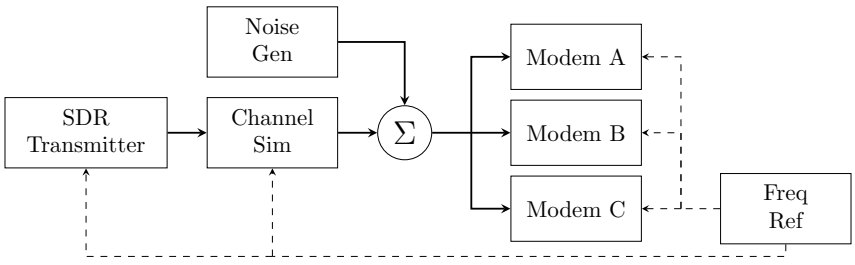

Figure 3: Laboratory test setup showing the path of RF signals (solid) and 10 MHz frequency reference (dashed) between instruments.

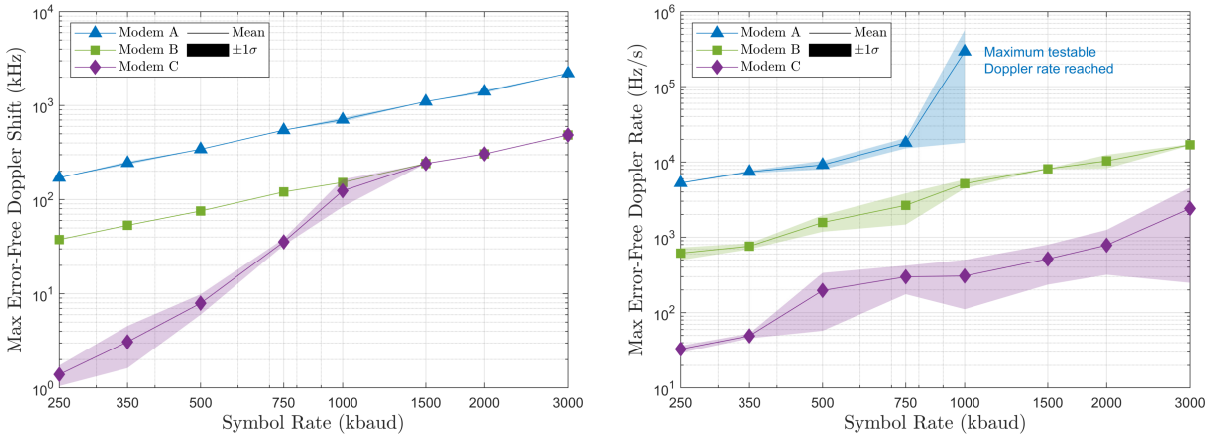

(a) (b)

Figure 4: Maximum error-free modem performance as a function of Doppler (a) shift and (b) rate. Statistics over 10 trials. For some modems, standard deviation (shaded area) is too small to be visible.

For rate characterization, linear frequency sweeps were generated at a large number of candidate Doppler rates. Sweeps were typically 60 seconds, except for very high rates which required a shorter duration to keep the starting and stopping frequencies within a reasonable range. Profiles were kept to a minimum duration of 5 seconds (which determined the maximum testable Doppler rate). After the transmitter was turned on, each modem was given 60 seconds to lock to the frequency offset which started the sweep. Once locked the sweep was run. At the end of the profile errors were checked. If no errors occurred during the sweep, the rate of the linear sweep was increased and the process repeated until errors appeared. Again ten trials were run. Results are shown in Fig. 4b.

Using these results along with the worst-case Doppler shift and rates in Fig. 2 we can estimate the lowest error-free symbol rate each modem can achieve (Table 1). We use interpolation to estimate between collected datapoints. We analyze both Doppler shift and rate to find the limiting factor, though in the cases considered here minimum baud rate is dictated by the Doppler shift. While one modem was able to operate down to 1 Mbaud without compensation, the others required a minimum 5 Mbaud to guarantee error-free transfer.

Link	Modem A	Modem B	Modem C
ISS $\rightarrow$ GEO	1.06	4.68	4.70
ISS $\rightarrow$ MEO	0.98	4.33	4.35
SSO $\rightarrow$ GEO	1.09	4.83	4.85
SSO $\rightarrow$ MEO	1.16	5.11	5.13

Table 1: Estimated minimum error-free symbol rate (Mbaud) under uncorrected Doppler conditions.

4 Theory of Operation

Conceptually, the spacecraft-side compensation process (Fig. 5) is straightforward. The transmit frequency of the radio is shifted by $-\Delta f_c$ (opposite of the anticipated Doppler shift). The two shifts cancel out and the signal is received at the desired frequency f_c. Compensation can also be applied in the spacecraft's receive direction following the same process. We begin with an estimate of the Doppler shift throughout the relay contact (i.e. the Doppler profile). This can be computed on the spacecraft's general purpose processor (GPP) using a lightweight onboard orbit propagation engine as in [6]. The inverse of this Doppler profile is used on the radio's field-programmable gate array (FPGA) to control the center frequency with precise timing.

We desire a highly lightweight design which uses minimal FPGA memory and logic resources. The raw estimated profile can contain a large number of individual points, which would require large storage resources onboard the FPGA. Non-linear interpolation methods used to approximate the entire curve from a subset of points are costly to implement on the FPGA fabric. We therefore break the profile curve into sections, and fit a piecewise linear slope to each section as illustrated in Fig. 6. Only the starting frequency and the slope of the line segment must be passed to the FPGA. Digital logic implements a simple linear frequency sweep, allowing for a lightweight implementation. Clearly, the piecewise linear approximation of a non-linear Doppler curve will cause error but this can be made negligible by choosing a reasonably small update rate. For the profiles in Fig. 2, a timestep of 1 s will produce error due to nonlinear approximation of less than 10 Hz.

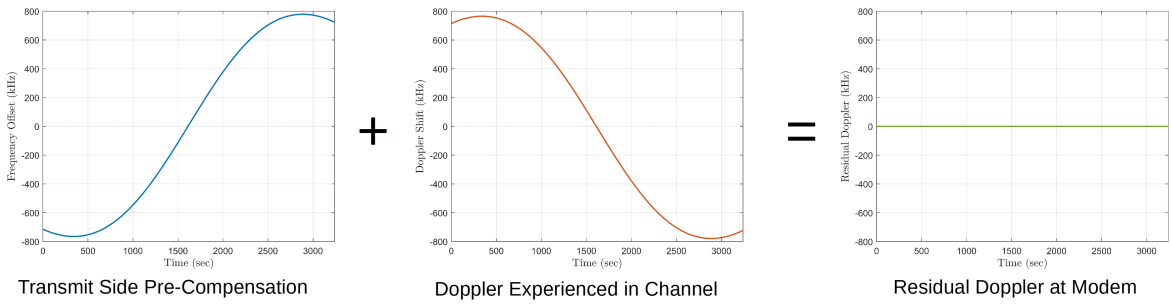

Figure 5: Conceptual overview of Doppler pre-compensation process.

Frequency offsets are accomplished on the FPGA by mixing the transmit-side baseband signal with the output of a numerically-controlled oscillator on the FPGA. The oscillator's frequency is set by a frequency control word ψ calculated as

$$\psi = \left\lfloor \frac{2^{n_{\text{fcw}}} f_c}{f_s} \right\rceil \tag{2}$$

where f_s is the FPGA clock frequency, n_{fcw} is the number of bits in the fixed-point representation of ψ, and the $\lfloor \cdot \rceil$ operation rounds to the nearest integer. If the value of ψ does not change, the center frequency of the transmitted signal will remain constant. Increasing ψ by a fixed value at regular intervals will produce a linear frequency sweep with a fixed slope.

4.1 GPP Calculation

To approximate the non-linear Doppler pre-compensation profile of duration t_{profile}, we will update the slope every t_{update} seconds. Every t_{step} seconds, we will either increment ψ by 1, decrement ψ by 1, or leave it unchanged. The number of times ψ will be modified within t_{update} is given by

$$n_{\text{update},i} = \left\lfloor \frac{t_{\text{update}}/t_{\text{step}}}{\psi_{i+1} - \psi_i} \right\rceil, \quad i \in \{0, \lfloor t_{\text{profile}}/t_{\text{update}} \rceil\} \tag{3}$$

where ψ_i is the frequency control word at the start of the linear sweep interval (or start of the pass if $i = 0$) and ψ_{i+1} is the desired at the end of the interval, t_{update} seconds later. The direction of the update (increasing or decreasing) is determined by $\text{sgn}(n_{\text{update}})$. The magnitude of n_{update} will determine the slope (lower magnitudes produce a steeper slope). The generation of $n_{\text{update},i}$, $i \in \{0, \lfloor t_{\text{profile}}/t_{\text{update}} \rceil\}$ takes place on the GPP before the pass begins. The GPP uses a timed process to transfer $n_{\text{update},i}$ to the FPGA every t_{update} seconds. In real hardware, the update will actually be passed every $t_{\text{update}} \pm t_{\text{error}}$ seconds where t_{error} is a processor-dependent inaccuracy in the software timer.

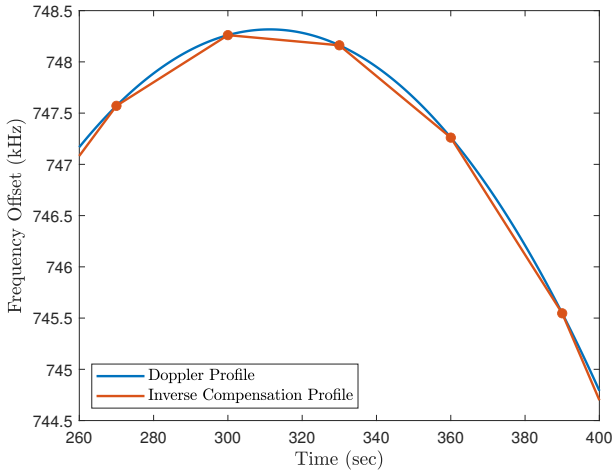

Figure 6: Linear approximation of the non-linear Doppler curve by using fixed line segments each 30 s in duration. Timesteps exaggerated for illustration, 1 s is a more typical value.

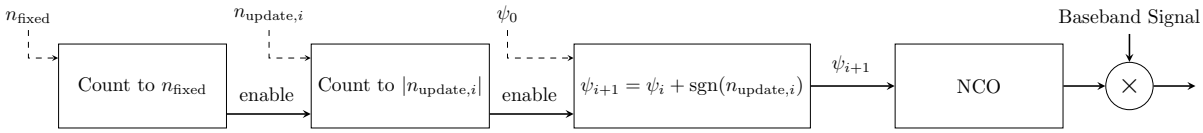

Figure 7: FPGA logic to generate a linear frequency sweep from a frequency control word and update rate. The generated sweep is mixed with the transmit signal to produce a frequency offset.

4.2 FPGA Calculation

The FPGA logic (Fig. 7) begins with a counter which produces an enable signal every t_{step} seconds by counting from 0 to $n_{\text{fixed}} = \lfloor t_{\text{step}} \cdot f_s \rceil$. A second counter, enabled by the first, will count from 0 to $|n_{\text{update},i}|$. This second counter enables the update of ψ. The value of n_{fixed} effectively inversely scales $n_{\text{update},i}$ and should be set small as possible giving more bits to represent the slope. However, we must ensure $n_{\text{update},i}$ does not overflow.

At the start of the pass, ψ_i is initialized to ψ_0. Every $t_{\text{step}} \cdot n_{\text{update},i}$ seconds, the frequency control word is adjusted by $\text{sgn}(n_{\text{update},i})$. The remainder of the process uses existing numerically-controlled oscillator (NCO) logic on the FPGA. A phase accumulator is driven by ψ_i which in turn provides an address to a sine/cosine look up table. The NCO outputs mix with the complex baseband signal to produce a transmit signal at the desired frequency offset.

5 Error Sources

In this section we list three principal sources of error resulting in residual Doppler at the receiver and investigate each in turn.

5.1 Timer Jitter

Fig. 8 shows a characterization the timing error of two flight-capable single-board computers and the Vadatech unit used for laboratory experiments. A software timer fires every 1 s, writes a new slope to the FPGA, and records the processor's current time with nanosecond precision. We observe the timing error following a normal distribution with zero mean and variance on the order of 100 ns. Increased software load may degrade the timing accuracy of the GPP. If this becomes a problem, it will not take much additional FPGA resources to store the approximately 3,000 points which make up the compensation profile at 1 s timestamps on the FPGA.

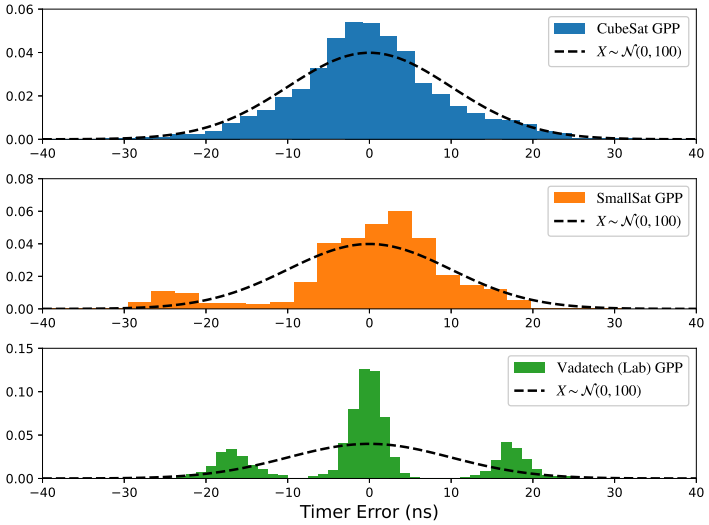

Figure 8: Measured error of a 1 s timer on flight-capable GPPs and the Vadatech GPP used in lab experiments. Error appears to follow a normal distribution. Statistics taken over one hour.

Algorithm 1: Compensation Profile Generation

$n_{\text{gpp}} \leftarrow \lceil t_{\text{profile}}/t_{\text{update}} \rceil$
Convert $\{\Delta f_{c,0}, \Delta f_{c,n_{\text{gpp}}}\}$ profile to $\{\psi_0, \psi_{n_{\text{gpp}}}\}$
$\psi_{\text{actual}} \leftarrow \psi_0$
for $i \in n_{\text{gpp}}$ **do**
  $n_{\text{update},i} \leftarrow \lfloor (t_{\text{update}}/t_{\text{step}})/(\psi_{i+1} - \psi_i) \rceil$
  for $j \in \lfloor t_{\text{update}}/t_{\text{step}} \rfloor$ **do**
    $\psi_{\text{actual}} \leftarrow \psi_{\text{actual}} + \text{sgn}(n_{\text{update},i})$
  $\Delta\psi \leftarrow \psi_{\text{actual}} - \psi_{i+1}$
  if $(\Delta\psi \neq 0)$ **then**
    $n_{\text{update},i} \leftarrow \lfloor (t_{\text{update}}/t_{\text{step}})/(\Delta\psi) \rceil$

5.2 Step Rounding Error

In this section, we denote the ideal points as ψ_i and their actual value in the FPGA as ψ'_i. The error ϵ_i between the two comes from the rounding operation in (3) and the floor operation in (4). After the interval t_{update}, the updated frequency control word will be

$$\psi'_{i+1} = \psi_i + \left\lfloor \frac{t_{\text{update}}/t_{\text{step}}}{n_{\text{update,i}}} \right\rfloor + \sum_{j<i} \epsilon_j \tag{4}$$

Since the prior value of ψ_i is the starting point for ψ_{i+1}, error accumulates each interval. We compensate for this by periodically adjusting the value of $n_{\text{update},i}$ to minimize $\epsilon_{i+1} = (\psi'_{i+1} - \psi_{i+1})$ as in Algorithm 1.

5.3 Ephemeris Uncertainty

Accuracy of the predicted Doppler profile depends on position knowledge of the user spacecraft and relay satellite. Mismatch between the spacecraft's assumed and actual position will produce a misalignment of t_{offset} seconds in the compensation profile and result in residual Doppler at the receiver. We assume the spacecraft's position knowledge is derived from an onboard GPS receiver such as [7] which has an average position uncertainty of 6 km in LEO. The offset can be calculated using Earth's radius r_E, standard gravitational parameter μ_E, and the orbital distance h_{orb}

$$t_{\text{offset}} = \sqrt{\frac{(r_E + h_{\text{orb}})}{\mu_E}} \cdot 6\text{km} \tag{5}$$

which results in an average offset of 782 ms and 790 ms for the ISS and SSO orbits, respectively.

6 Results

The Doppler compensation module was implemented on the Vadatech SDR's Virtex-7 FPGA. The module was clocked to f_s = 200 MHz and n_{fcw} = 29 bits were used for fixed-point representation of ψ. As shown in Table 2, minimal FPGA resources (∼1% or less) were used. The piecewise linear sweep logic is small compared to the NCO and mixer. In some SDRs which operate at an intermediate frequency, this mixing logic may already be required in the design. In this case, addition of the Doppler compensation module will require no additional block random access memory (BRAM) or digital signal processing (DSP) blocks.

Resource	Sweep Logic Only	NCO + Mixer	Total
LUTs	290	701	991 (0.23%)
Registers	184	2147	2331 (0.27%)
DSPs	0	40	40 (1.1%)
BRAMs	0	4	4 (0.27%)

Table 2: Resources utilized by the Doppler compensation module.

Performance of the module was characterized using the worst-case Doppler profiles in Fig. 2 and the test setup in Fig. 3. Frame error statistics were collected from three modems as the entire pass was emulated using the channel simulator. Modem A also provided carrier frequency offset estimates which were used to measure the residual Doppler after compensation.

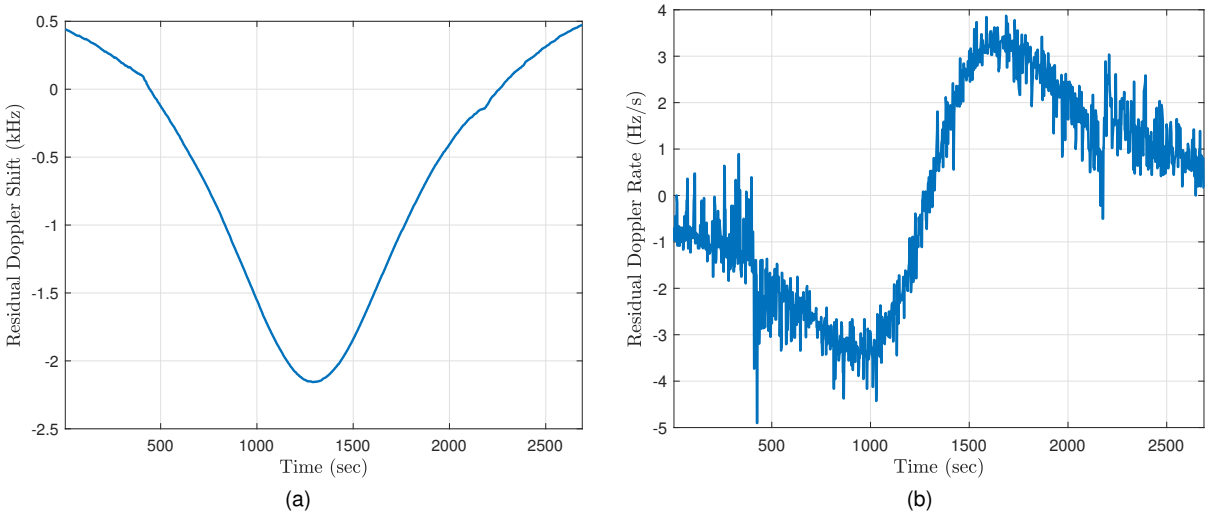

Figure 9: Residual Doppler (a) shift and (b) rate, as measured by Modem A, after compensation was applied to the SSO → MEO pass.

Fig. 9 shows residual Doppler in the SSO → MEO pass, which represents the most difficult link considered. A symbol rate of 250 kbaud was used, which is the minimum rate supported by all modems. Link margin was set to 3 dB. We observe a negligible residual rate and a residual shift of 2.1 kHz - a reduction of 375x compared to the uncompensated Doppler shift. All modems were locked within 40 s and afterwards accumulated no errors for the duration of the 45 minute profile. Table 3 summarizes results for the other links considered.

Link	Max Doppler (kHz)	Residual (kHz)	Lock Time (s)	Frame Errors
ISS → GEO	756	1.35	13, 27, 28	0, 0, 0
ISS → MEO	699	1.44	42, 12, 19	0, 0, 0
SSO → GEO	780	1.40	40, 15, 33	0, 0, 0
SSO → MEO	826	2.16	10, 34, 33	0, 0, 0

Table 3: Experimental results under different Doppler profiles. Symbol rate was 250 kbaud and link margin was 3 dB. Lock Time and Errors are listed for Modems A, B, and C (in that order). Residual Doppler comes from the frequency offset estimator on Modem A. Frame error statistics were calculated from beginning of lock through the end of the profile.

7 Conclusion

We believe this development offers an important additional option within the tradespace for low-rate communications. Spacecraft could use lower-frequency (e.g. L-band, C-band) services with correspondingly lower Doppler effects. However, this involves the mass penalty of flying a second radio terminal and antenna aperture. NASA could require commercial service providers it does business with to provide ground-side Doppler compensation. However, this service would not be utilized by most terrestrial customers and would likely result in associated costs largely being passed on to space missions. Finally, more complex methods of spacecraft-side compensation could be implemented to further reduce residual Doppler. However, this would require more resources on FPGAs that are likely already heavily utilized. In this work, we have demonstrated our proposed spacecraft-side compensation technique is a viable method to reduce Doppler effects by over two orders of magnitude. The residual Doppler is low enough that unmodified provider modems can close links down to kbaud rates in several common spacecraft orbits.

References

[1] Piasecki, M., Downey, J., Pham, N., et al.: 'Development and demonstration of a wideband RF user terminal for roaming between ka-band relay satellite networks'. In: Proc. 38th International Communications Satellite Systems Conference (ICSSC). (Arlington, VA, 2021).

[2] Heckler, G., Younes, B., Mitchell, J., et al.: 'NASA's wideband multilingual terminal efforts as a key building block for a future interoperable communications architecture'. In: Proc. 26th Ka and Broadband Communications Conference. (Arlington, VA, 2021).

[3] Moakkit, H.: 'O3b an innovative way to use ka band'. In: ITU Workshop on the efficient use of the spectrum/orbit resource. (Limassol, Cyprus, 2014).

[4] Downey, J., Evans, M., Tollis, N. 'DVB-S2 experiment over NASA's space network'. (NASA Glenn Research Center, 2017). NASA/TM—2017-219524

[5] 'Digital video broadcasting (DVB); second generation'. (European Telecommunications Standards Institute, 2009). ETSI EN 302 307 v1.2.1

[6] Gannon, A., Gemelas, C., Paulus, S., et al.: 'An augmented ground station architecture for spacecraft-initiated communication service requests'. In: 16th International Conference on Space Operations (SpaceOps). (Cape Town, South Africa, 2021).

[7] 'Cubesat kit GPSRM 1 GNSS receiver module'. (Pumpkin, Inc., 2022). Revision D